Structural Chemistry
https://doi.org/10.1007/s11224-020-01697-4

ORIGINAL RESEARCH

Molecular modeling investigation of adsorption of Zolinza drug on surfaces of the $B_{12}N_{12}$ and $Al_{12}N_{12}$ nanocages

Masoome Sheikhi[1] · Yavar Ahmadi[2] · Sadegh Kaviani[3] · Siyamak Shahab[4,5,6]

Received: 30 September 2020 / Accepted: 2 December 2020

Abstract

In the current work, the adsorption of Zolinza (ZOL) drug on $B_{12}N_{12}$ and $Al_{12}N_{12}$ nanocages was investigated using density functional theory (DFT) and time-dependent DFT (TDDFT) calculations at the M06-2X/6-31+G* level of theory in the solvent water. We have studied the adsorption effect of the ZOL on the bond lengths and electronic properties such as frontier molecular orbital (FMO) analysis, dipole moment, and excited states of $B_{12}N_{12}$ and $Al_{12}N_{12}$ nanocages. The UV absorption spectra were computed to study the changes that occur during the adsorption process of ZOL on surface $B_{12}N_{12}$ and $Al_{12}N_{12}$ nanocages. Natural bond orbital (NBO) analysis revealed a charge transfer from the oxygen and nitrogen atoms of ZOL to the B and Al atoms of nanocages. The analysis of the LOL and ELF was shown the B-N and B-O bonds are greater than the other bonds, representing higher electron density localization and stronger covalent characteristic. It is found that the applied $B_{12}N_{12}$ fullerene can be suitable as a drug carrier for the delivery of ZOL drug.

Keywords Zolinza · $B_{12}N_{12}$ nanocage · $Al_{12}N_{12}$ nanocage · DFT · TD-DFT

Introduction

The epigenome is defined as a record of the chemical corrections of DNA molecule and histone proteins that do not change the sequence of DNA strands. DNA methylation, histone acetylation, and chromatin remodeling are examples of epigenetic changes [1]. These epigenetic changes are important in the regulation of gene expression and cellular phenotype [1]. Based on human studies, excessive histone deacetylases (HDAC) activity mediates the deacetylation of histones, thereby downregulating the expression of tumor suppressor genes, such as p21WAF1 [2–5]. HDAC inhibitors have an anti-tumor effect on various tumor cell lines in vitro and in vivo in humans and dogs [3–8]. HDAC inhibitors induce the acetylation of deacetylated histones and restore the expression of tumor suppressor genes, potentially resulting in an anti-tumor effect [3, 4]. HDAC enzymes remove acetyl groups with histone acetyltransferases (HAT). Related toxicities for HDAC are low [9, 10]. Vorinostat (suberoylanilide hydroxamic acid) with trade name Zolinza (ZOL) (Scheme 1) is a HDAC inhibitor clinically approved for the treatment of human cutaneous T cell lymphoma [11]. Based on studies, Zolinza has an anti-tumor effect on various hematological and solid tumors in vitro and in vivo such as ovarian cancer cells and xenografts [12], colon cancer

✉ Masoome Sheikhi
m.sheikhi2@gmail.com

Yavar Ahmadi
Y.Ahmadi@cfu.ac.ir

Sadegh Kaviani
sadegh_kaviani2000@yahoo.com

Siyamak Shahab
siyamak.shahab@yahoo.com

[1] Young Researchers and Elite Club, Gorgan Branch, Islamic Azad University, Gorgan, Iran

[2] Department of Basic Sciences, Farhangian University, Tehran, Iran

[3] Department of Chemistry, Faculty of Science, Ferdowsi University of Mashhad, Mashhad, Iran

[4] Belarusian State University, ISEI BSU, Minsk, Republic of Belarus

[5] Institute of Physical Organic Chemistry, National Academy of Sciences of Belarus, 13 Surganov Str., 220072 Minsk, Republic of Belarus

[6] Institute of Chemistry of New Materials, National Academy of Sciences of Belarus, 36 Skarina Str., 220141 Minsk, Republic of Belarus

Published online: 07 January 2021

Scheme 1 Chemical structural of Zolinza (ZOL)

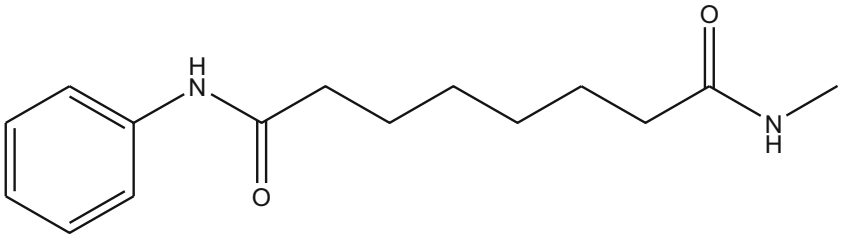

cells [13], breast cancer [14], and lung cancer [15, 16]. It is only one of four HDAC inhibitors approved for clinical use by the FDA (Food and Drug Administration, US) [17, 18].

In recent years, nanotechnology has been used widely in the field of medicine and drug delivery [19–21]. A lot of studies have been done on the carbonic and non-carbonic nanostructures such as nano-tubes [22–24], fullerene-like nanocages [25, 26], and nano-sheets [27] due to their unique chemical, physical, and surface properties. Seifert and co-workers have reported that the nanocage (B_nN_n) with $n = 12$ ($B_{12}N_{12}$) is the most stable structure, which is consisted of six tetragon rings and eight hexagon rings [28]. $B_{12}N_{12}$ and $Al_{12}N_{12}$ nanocages are the most stable structures, which have been synthesized by Oku and co-workers [29] and Liu and co-workers [30], respectively. They have unique physicochemical properties such as high thermal conductivity, chemical stability, wide band gap, and oxidation resistance [31, 32]. According to studies, $Al_{12}N_{12}$ nanocage is the most stable structure and is therefore ideal inorganic fullerene-like nanocage [33]. Adsorption of many molecules on the surface of $B_{12}N_{12}$ and $Al_{12}N_{12}$ nanocages has been studied using theoretical methods. Based on the report of Vessally and co-workers, $B_{12}N_{12}$ and $B_{11}N_{12}Al$ nanocages can act as a suitable candidate for the adsorption of aspirin drug [34]. Bahrami and co-workers have investigated the adsorption of some nonpolar X_2 compounds (X = Li, Be, B, N, O, F, Cl, Br, I) on the $B_{12}N_{12}$ nanocages [35]. The studies have shown that $B_{12}N_{12}$ nanocage has given considerable response to other X_2 molecules except for N_2 and F_2. According to the studies of Yourdkhani and co-workers, the $B_{12}N_{12}$ nanoclusters have a high ability in the formation of complexes with hydrogen halides [36]. Shokuhi Rad and co-workers [37] have reported the adsorption of CH_3F and CH_3Cl on the surfaces of $Al_{12}N_{12}$ and $Al_{12}P_{12}$ nanocages. Their results have shown that $Al_{12}N_{12}$ can be considered as a better biosensor in comparison to $Al_{12}P_{12}$. Recently, we reported adsorption of solariamfetol drug on the surface of $B_{12}N_{12}$ nanocage [38].

In this research, we studied comparison of the adsorption effect of Zolinza (ZOL) drug over $B_{12}N_{12}$ and $Al_{12}N_{12}$ nanocages based on geometries, energies, electronic properties, frontier molecular orbital (FMO), excited states, and QTAIM analysis to determine suitable drug delivery for ZOL drug by DFT and TD-DFT methods. We hope that the results of our study can be useful for designing an appropriate and novel carrier for the delivery of Zolinza drug.

Computational methods

In this work, we have studied the adsorption ZOL drug on the $B_{12}N_{12}$ and $Al_{12}N_{12}$ nanocages by theoretical calculations. The quantum chemical calculations, geometry optimizations, the density of states (DOS), and FMO analysis were carried out using the DFT method (M062X/6-31+G*) by the Gaussian 09W program [39] in the solvent water. The Polarized Continuum Model (PCM) [40] was used for the calculations of the solvent effect. The adsorption energies (E_{ads}) [27] of ZOL molecule over $B_{12}N_{12}$ and $Al_{12}N_{12}$ nanocages are calculated by the following equation:

$$E_{ads} = E_{ZOL/nanocage} - \left[E_{ZOL} + E_{nanocage}\right] \quad (1)$$

in which $E_{ZOL/nanocage}$ is the energy of ZOL adsorbed over the free nanocages. E_{ZOL} displays the energy of an isolated ZOL drug and $E_{nanocage}$ is the energy of the free nanocage. The thermodynamic parameters and electronic properties of the investigated molecules such as E_{HOMO}, E_{LUMO}, the energy gap between LUMO and HOMO, and natural bond orbital (NBO) analysis [41] were calculated. The optimized molecular structures and the molecular orbital's graphs were visualized by GaussView 05 program [42]. The GaussSum program was used to calculate the density-of-state plots (DOS) [43]. TD-DFT method [44] was used for the calculation of the electronic transitions of the title compounds. The quantum theory of atoms in molecule (QTAIM) analysis [45] was carried out by MultiWFN 3.1 [46].

Results and discussion

Optimized structures and thermodynamic parameters

The interactions of ZOL with $B_{12}N_{12}$, and $Al_{12}N_{12}$ fullerenes are investigated in five molecular orientations (models **A**, **B**, **C**,

Table 1 Calculated average bond lengths (Å) and bond angles (°) of ZOL adsorbed on the $B_{12}N_{12}$ and $Al_{12}N_{12}$ nanocages in the solvent water

Compound	Model	B-N	Al-N	N-B-N	N-Al-N
$B_{12}N_{12}$	-	1.50	-	124.23	-
$Al_{12}N_{12}$	-	-	1.87	-	123.00
ZOL/$B_{12}N_{12}$	A	1.56	-	117.58	-
	B	1.58	-	115.99	-
	C	1.64	-	113.72	-
	D	1.56	-	115.74	-
	E	1.60	-	113.61	-
ZOL/$B_{12}N_{12}$	A	-	1.90	-	119.23
	B	-	1.90	-	117.71
	C	-	1.91	-	119.44
	D	-	1.89	-	118.87
	E	-	1.90	-	124.17

D, and **E**) using DFT calculations. The optimized structures of ZOL, $B_{12}N_{12}$, and $Al_{12}N_{12}$ nanocages and the ZOL/$B_{12}N_{12}$, and ZOL/$Al_{12}N_{12}$ (models **A**–**E**) complexes are presented in Figs. 1, 2, and 3. As can be seen from Figs. 2 and 3, the B17 atom of $B_{12}N_{12}$ nanocage and the Al52 atom of $Al_{12}N_{12}$ nanocage interact with the oxygen and nitrogen of ZOL. The calculated geometrical parameters of the isolated nanocages and complexes are reported in Table 1. According to data in Table 1, the calculated B-N bond length and N-B-N bond angles of isolated $B_{12}N_{12}$ nanocage are 1.50 Å and 124.23° respectively; whereas at the models **A**, **B**, **C**, **D**, and **E** of ZOL/$B_{12}N_{12}$, these values change to 1.56 Å (117.58°), 1.58 Å (115.99°), 1.64 Å (113.72°), 1.56 Å (115.74°), and 1.60 Å (113.61°), respectively. The calculated Al-N bond length and N-Al-N bond angles of isolated $Al_{12}N_{12}$ nanocage are 1.87 Å and 123.00° respectively, whereas at the models **A**, **B**, **C**, **D**, and **E** of ZOL/$Al_{12}N_{12}$, these values change to 1.90 Å (119.23°), 1.90 Å (117.71°), 1.91 Å (119.44°), 1.89 Å (118.87°), and 1.90 Å (124.17°), respectively. The B-N and Al-N bond lengths increase after the interaction of ZOL with nanocages. According to the results, ZOL has the strongest interaction with $B_{12}N_{12}$ nanocage rather than $Al_{12}N_{12}$ nanocage.

The thermochemical parameters including the sum of electronic and thermal energies ($E + T$), the sum of electronic and thermal enthalpies ($E + H$), the sum of electronic and thermal free energies ($E + G$), the sum of electronic and zero-point energies (ZPE), and entropy (S) of the ZOL drug, and $B_{12}N_{12}$ and $Al_{12}N_{12}$ nanocages, and the adsorbed ZOL on the $B_{12}N_{12}$ and $Al_{12}N_{12}$ nanocages (models **A**, **B**, **C**, **D**, and **E**) are calculated using M06-2X/6-31+G* level of theory. The calculated results are summarized in Table 2. With the adsorption of the ZOL on $B_{12}N_{12}$ and $Al_{12}N_{12}$ nanocages, the energy values of Thermal, Gibbs, Enthalpy, and ZEP decrease. The ZOL/$Al_{12}N_{12}$ complexes

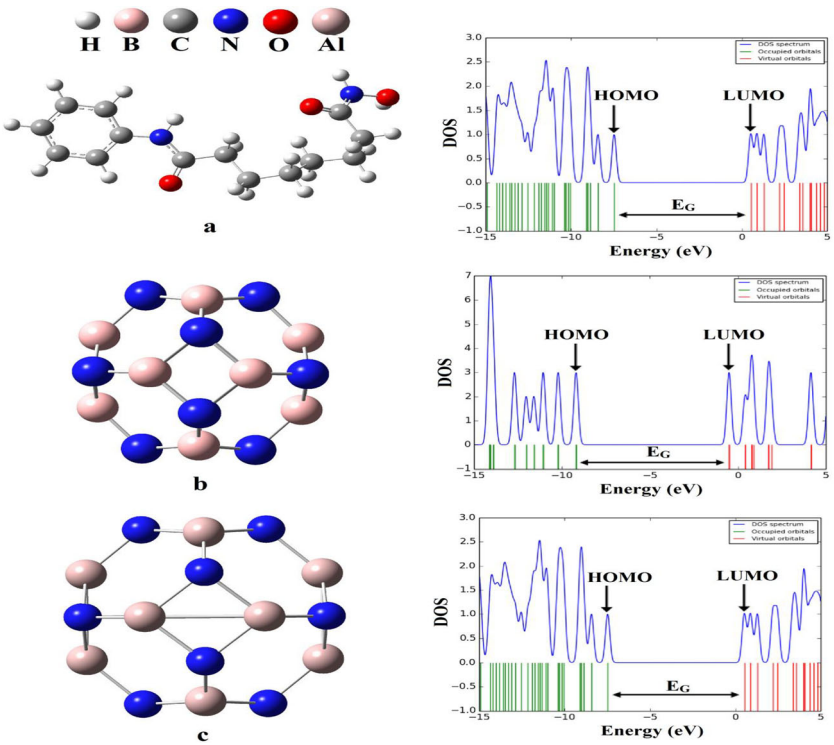

Fig. 1 The optimized geometry and DOS plots of the ZOL molecule and $B_{12}N_{12}$ and $Al_{12}N_{12}$ nanocages

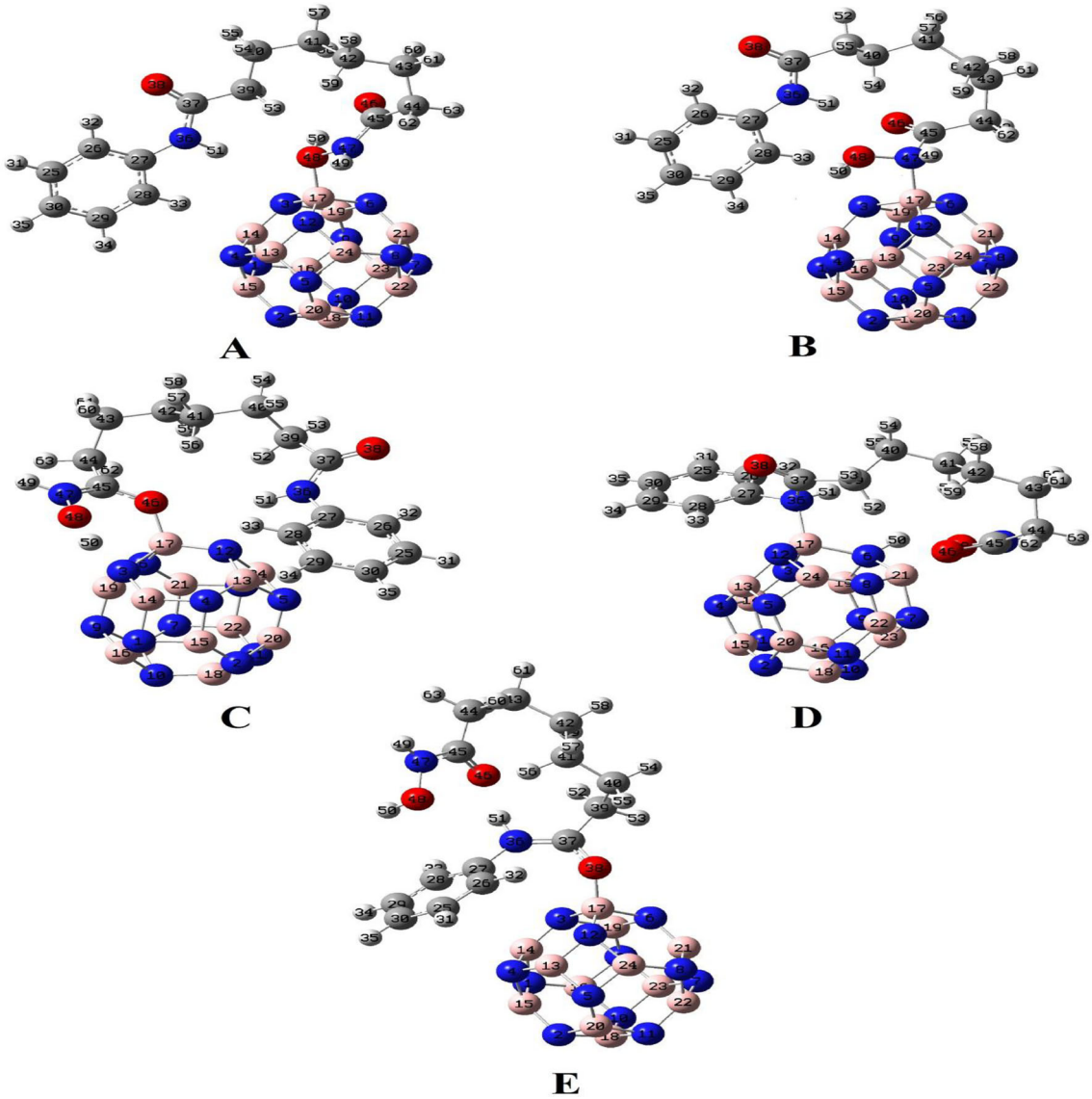

Fig. 2 The optimized geometry of the ZOL/$B_{12}N_{12}$ complexes (models **A**–**E**)

are the most negative compared to the ZOL/$B_{12}N_{12}$ complexes. According to the data in Table 2, the calculated ΔG values show that the complex formation process is spontaneous. The ΔH values of the adsorption process display the adsorption of ZOL drug on $B_{12}N_{12}$ and $Al_{12}N_{12}$ nanocages are exothermic.

Electronic properties

We studied the effects of the adsorption of the ZOL molecule on the electronic properties of $B_{12}N_{12}$ and $Al_{12}N_{12}$ nanocages. The calculated results are summarized in Table 3.

The adsorption energy of ZOL on $B_{12}N_{12}$ nanocage in models **A**, **B**, **C**, **D**, and **E** is calculated about − 1.27, − 1.49, − 2.09, − 2.74, and − 2.23 eV with the relax distances of 1.596, 1.643, 1.511, 1.638, and 1.507 Å, respectively. The calculated values of adsorption energy of ZOL on $Al_{12}N_{12}$ nanocage in models **A**, **B**, **C**, **D**, and **E** is about − 1.44, − 1.19, − 2.25, − 1.25, and − 2.50 eV with the relax distances of 1.940, 2.057, 1.865, 2.063, and 1.805 Å, respectively. It is found that the adsorption of ZOL drug on the $B_{12}N_{12}$ and $Al_{12}N_{12}$ nanocages is exothermic. The values of energy display that the adsorption of the ZOL on $B_{12}N_{12}$ and $Al_{12}N_{12}$ nanocages is chemisorption, and there is a potential interaction between the ZOL drug and two nanocages.

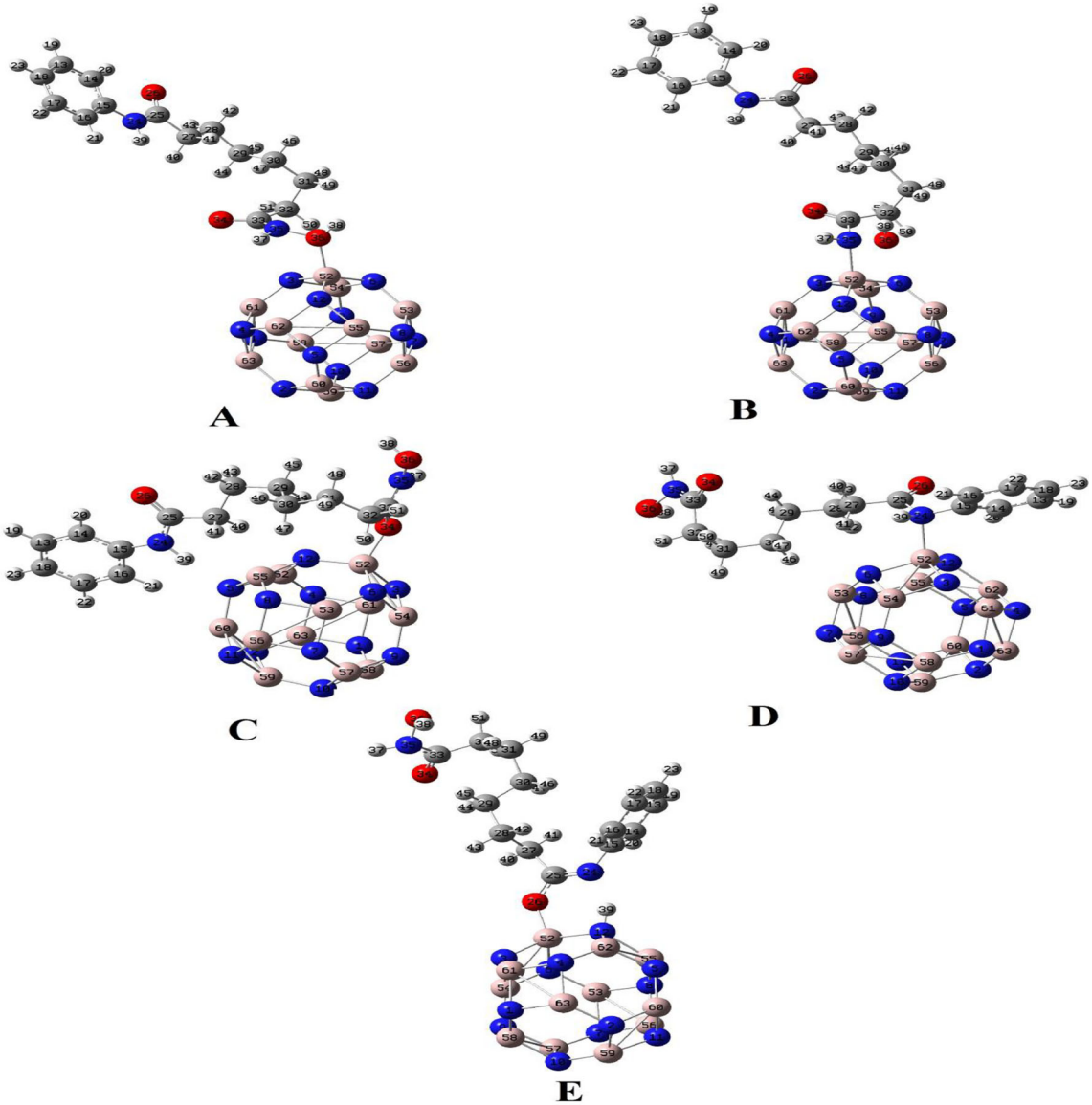

Fig. 3 The optimized geometry of the ZOL/$Al_{12}N_{12}$ complexes (models **A**–**E**)

The adsorption of the ZOL molecule has a significant effect on the dipole moment (D_M) of nanocages. The calculated values of D_M of isolated $B_{12}N_{12}$ and $Al_{12}N_{12}$ nanocages are 0.00 Debye, which is due to their symmetrical structure. The D_M values of ZOL/$B_{12}N_{12}$ and ZOL/$Al_{12}N_{12}$ increase rather than the free $B_{12}N_{12}$ and $Al_{12}N_{12}$ nanocages, which can be due to the considerable charge separation between the ZOL molecule and nanocages. On the other hand, the adsorption of ZOL drug over $B_{12}N_{12}$ and $Al_{12}N_{12}$ nanocages leads to increasing polarization in complexes due to the formation of polar bonds between the ZOL and the nanocages. The highest dipole moment is observed for model **E** of the ZOL/$B_{12}N_{12}$ complex (23.89 Debye). Also, the change of D_M shows a charge transfer between the ZOL drug and $B_{12}N_{12}$ and $Al_{12}N_{12}$ nanocages.

The frontier molecular orbital of the ZOL, $B_{12}N_{12}$, and $Al_{12}N_{12}$ nanocages and their complexes are shown in Figs. 4, 5, and 6. The HOMO orbital in $B_{12}N_{12}$ and $Al_{12}N_{12}$ nanocages is mostly focused on N atoms, while the LUMO orbital is localized on B and Al atoms (Fig. 4). The changes occur in HOMO and LUMO orbitals during the interaction of ZOL with nanocages. According to Fig. 5, the electron density of HOMO of models **A**, **B**, **C**, **D**, and **E** mainly focuses on the ZOL, while the LUMO orbital is

Table 2 The thermochemical parameters of the ZOL molecule, $B_{12}N_{12}$ and $Al_{12}N_{12}$ nanocages, and ZOL adsorbed on the $B_{12}N_{12}$ and $Al_{12}N_{12}$ and relative values of energies

Property	$E+G$ (Hartree)	$E+H$ (Hartree)	$E+T$ (Hartree)	ZPE (Hartree)	S (cal/mol.K)	ΔG	ΔH
ZOL	− 879.802	− 879.731	− 879.732	− 879.751	149.455	-	-
$B_{12}N_{12}$	− 955.428	− 955.382	− 955.383	− 955.393	96.566	-	-
Model **A**	− 1835.250	− 1835.157	− 1835.158	− 1835.188	196.175	− 0.02	− 0.044
Model **B**	− 1835.256	− 1835.165	− 1835.166	− 1835.195	192.630	− 0.026	− 0.052
Model **C**	− 1835.279	− 1835.189	− 1835.190	− 1835.219	190.348	− 0.049	− 0.076
Model **D**	− 1835.295	− 1835.210	− 1835.211	− 1835.239	180.086	− 0.065	− 0.097
Model **E**	− 1835.282	− 1835.192	− 1835.193	− 1835.223	188.061	− 0.052	− 0.079
$Al_{12}N_{12}$	− 3566.215	− 3566.149	− 3566.150	− 3566.170	137.906	-	-
Model **A**	− 4446.047	− 4445.931	− 4445.932	− 4445.972	244.819	− 0.03	− 0.051
Model **B**	− 4446.037	− 4445.921	− 4445.922	− 4445.962	243.388	− 0.02	− 0.041
Model **C**	− 4446.071	− 4445.961	− 4445.962	− 4446.002	232.918	− 0.054	− 0.081
Model **D**	− 4446.036	− 4445.923	− 4445.924	− 4445.964	238.155	− 0.019	− 0.043
Model **E**	− 4446.084	− 4445.971	− 4445.972	− 4446.012	239.624	− 0.067	− 0.091

$E+T$, the sum of electronic and thermal energies; $E+H$, the sum of electronic and thermal enthalpies; $E+G$, the sum of electronic and thermal free energies

Table 3 The calculated adsorption energy (E_{ad}), HOMO and LUMO energies, energy gap (E_G), dipole moment (D_M) of the ZOL, free $B_{12}N_{12}$ and $Al_{12}N_{12}$ nanocages, and corresponding complexes

Property	D_M/Debye	E/a.u.	E_{ads}/eV	E_{HOMO}/eV	E_{LUMO}/eV	E_G/eV	Point group
ZOL	6.74	− 880.087	-	− 7.47	0.52	6.95	C1
$B_{12}N_{12}$	0.00	− 955.522	-	− 9.19	− 0.51	8.68	T_h
Model **A**	8.22	− 1835.656	− 1.27	− 7.48	− 0.16	7.32	C1
Model **B**	9.10	− 1835.664	− 1.49	− 7.49	− 1.14	6.35	C1
Model **C**	13.87	− 1835.686	− 2.09	− 7.71	− 0.55	7.16	C1
Model **D**	14.40	− 1835.710	− 2.74	− 7.65	− 0.32	7.33	C1
Model **E**	23.89	− 1835.691	− 2.23	− 8.13	− 0.54	7.95	C1
$Al_{12}N_{12}$	0.00	− 3566.250	–	− 7.83	− 1.87	5.96	CS
Model **A**	6.46	− 4446.390	− 1.44	− 7.47	− 1.69	5.78	C1
Model **B**	5.76	− 4446.381	− 1.19	− 7.49	− 1.66	5.83	C1
Model **C**	10.55	− 4446.420	− 2.25	− 7.37	− 1.64	5.73	C1
Model **D**	4.84	− 4446.383	− 1.25	− 7.57	− 1.65	5.92	C1
Model **E**	9.37	− 4446.429	− 2.50	− 7.46	− 1.79	5.67	C1

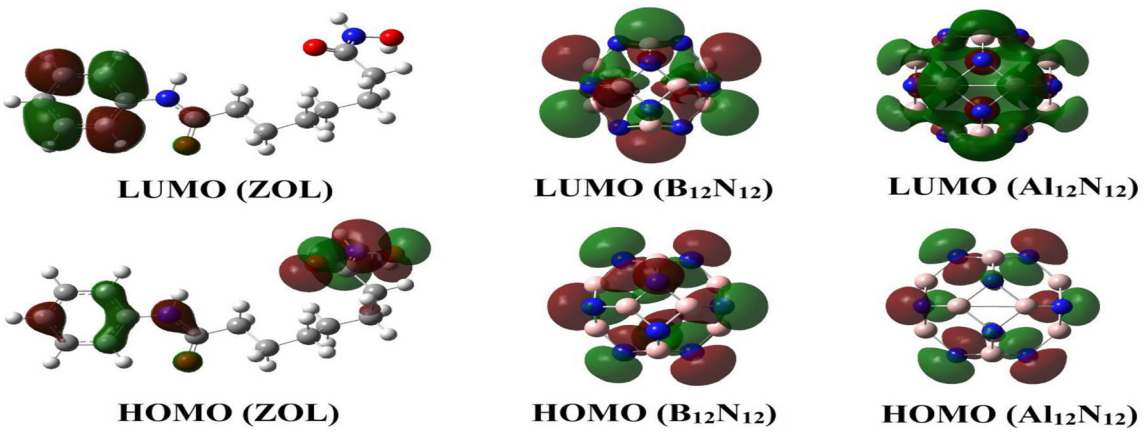

Fig. 4 The calculated HOMO and LUMO orbitals of the ZOL and $B_{12}N_{12}$ and $Al_{12}N_{12}$ nanocages

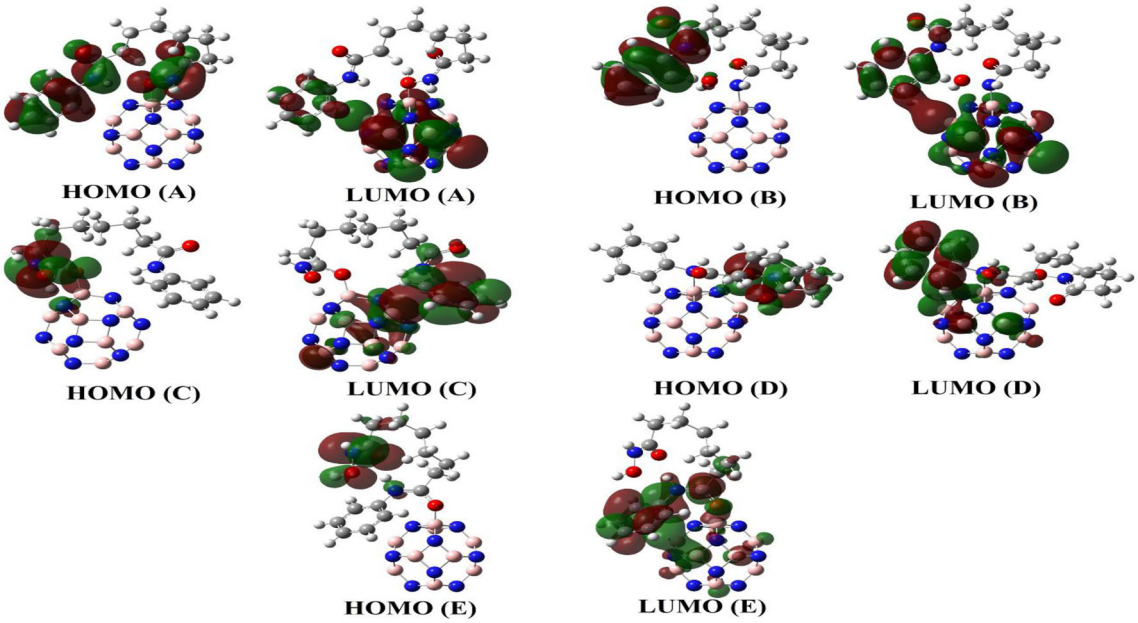

Fig. 5 The calculated HOMO and LUMO orbitals of the ZOL adsorbed on $B_{12}N_{12}$ and $Al_{12}N_{12}$ nanocages

distributed on both sections of ZOL and $B_{12}N_{12}$ nanocage. Figure 6 shows the HOMO and LUMO orbitals of ZOL/$Al_{12}N_{12}$ complexes. The HOMO orbital of states models **A**, **B**, **C**, **D**, and **E** mainly centralizes on the ZOL drug, while the LUMO orbital localize on $Al_{12}N_{12}$ nanocage.

As shown in Table 3, the energies of HOMO (LUMO) orbitals of $B_{12}N_{12}$ and $Al_{12}N_{12}$ nanocages are calculated about − 9.19 (− 0.51) and − 7.83 (− 1.87) eV. The energy values of HOMO (LUMO) for ZOL/$B_{12}N_{12}$ complexes is calculated about **A**: − 7.48 (− 0.16), **B**: − 7.49 (− 1.14), **C**:

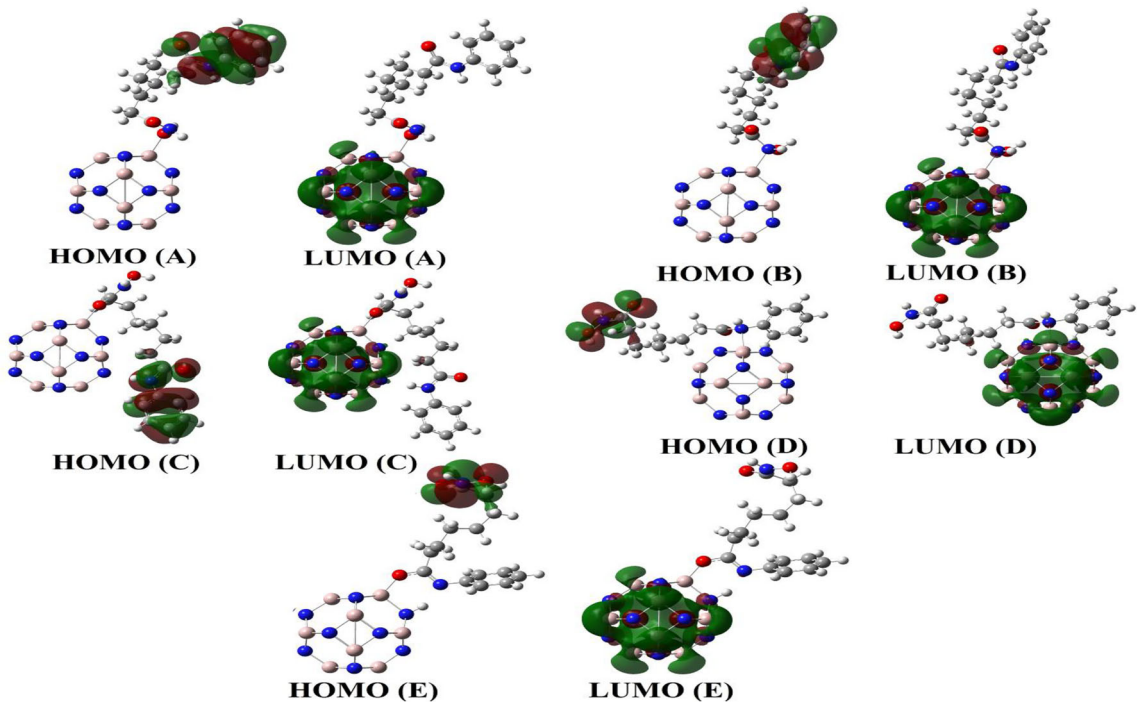

Fig. 6 The calculated HOMO and LUMO orbitals of the ZOL adsorbed on $Al_{12}N_{12}$ nanocage (models **A**–**E**)

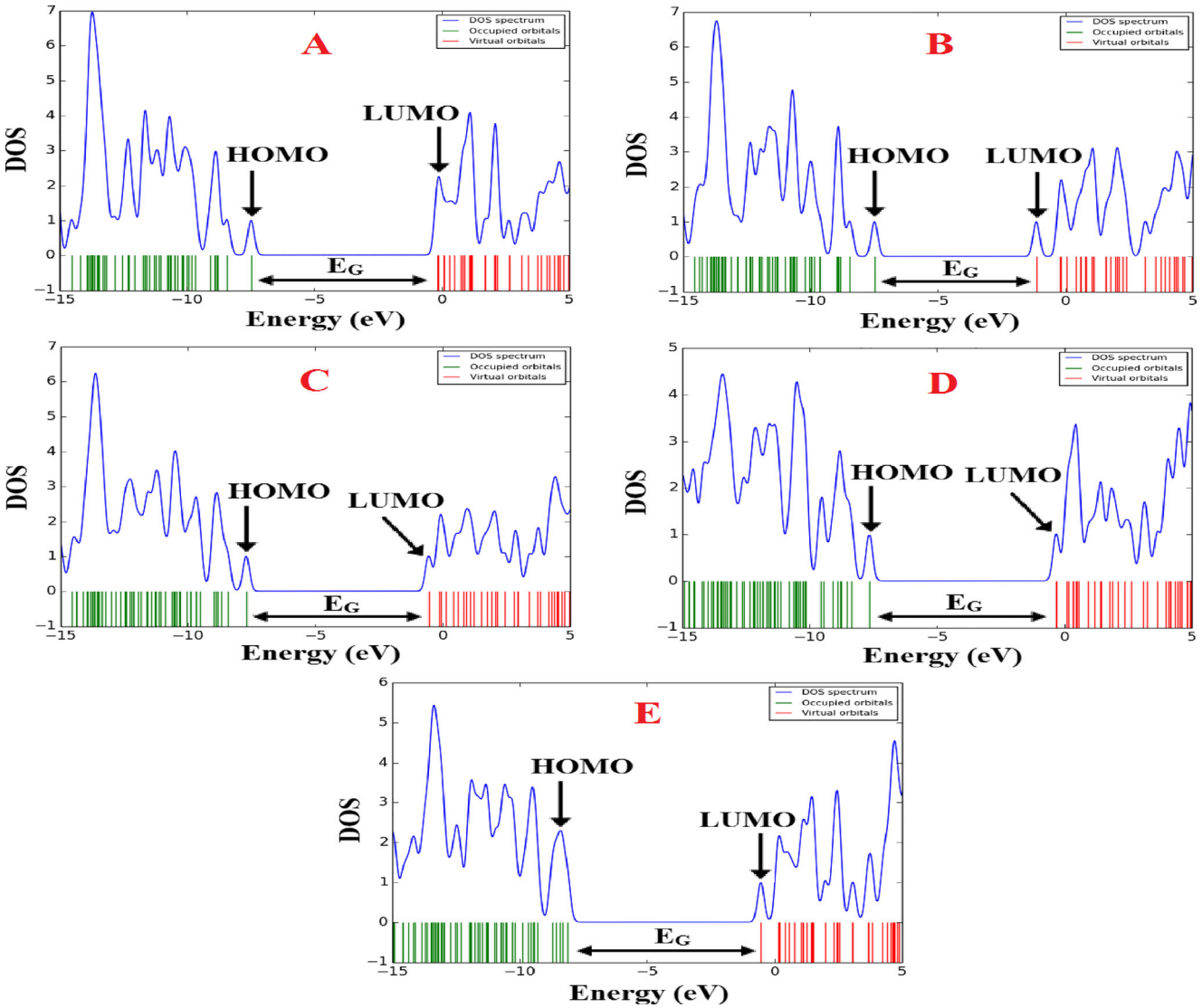

Fig. 7 DOS plots of the ZOL molecule and $B_{12}N_{12}$ and $Al_{12}N_{12}$ nanocages

−7.71 (−0.55), **D**: −7.65 (−0.32) **E**: −8.13 (−0.54), and for ZOL/$Al_{12}N_{12}$ complexes is calculated about **A**: −7.47 (−1.69), **B**: −7.49 (−1.66), **C**: −7.37 (−1.64), **D**: −7.57 (1.65) **E**: −7.46 (1.79). Thus, after the interaction of ZOL with $Al_{12}N_{12}$ nanocage, both HOMO and LUMO values shift to the less negative values, while after adsorption of ZOL on $B_{12}N_{12}$ nanocage, only the HOMO value shifts to the less negative value. The energy gap (E_G) for free $B_{12}N_{12}$ nanocage and models **A**, **B**, **C**, **D**, and **E** is calculated about 8.68, 7.32, 6.35, 7.16, 7.33, and 7.95 eV, and the E_G for free $Al_{12}N_{12}$ nanocage and models **A**, **B**, **C**, **D**, and **E** is obtained about 5.96, 5.78, 5.83, 5.73, 5.92, and 5.67 eV, respectively. Baei and co-workers have reported the E_G for $Al_{12}N_{12}$ nanocage about 3.92 eV and 3.85 eV using B3LYP method with various basis sets [47]. The E_G values are reduced during the adsorption process of ZOL on two nanocages; thus, conductivity increased which is an important parameter for use in electrochemical sensors. The $B_{12}N_{12}$ nanocage with the higher change in the E_G is the better candidate as a suitable electrochemical sensor in comparison to the $Al_{12}N_{12}$ nanocage. The adsorption of the ZOL from the head of the N24 atom (model **B**) on the surface of the $B_{12}N_{12}$ nanocage is more considerable in comparison to other models due to the lower E_G (6.35 eV).

The electronic density of state (DOS) plots of ZOL, free $B_{12}N_{12}$, and $Al_{12}N_{12}$ nanocages and their complexes are presented in Figs. 2, 7, and 8. The DOS

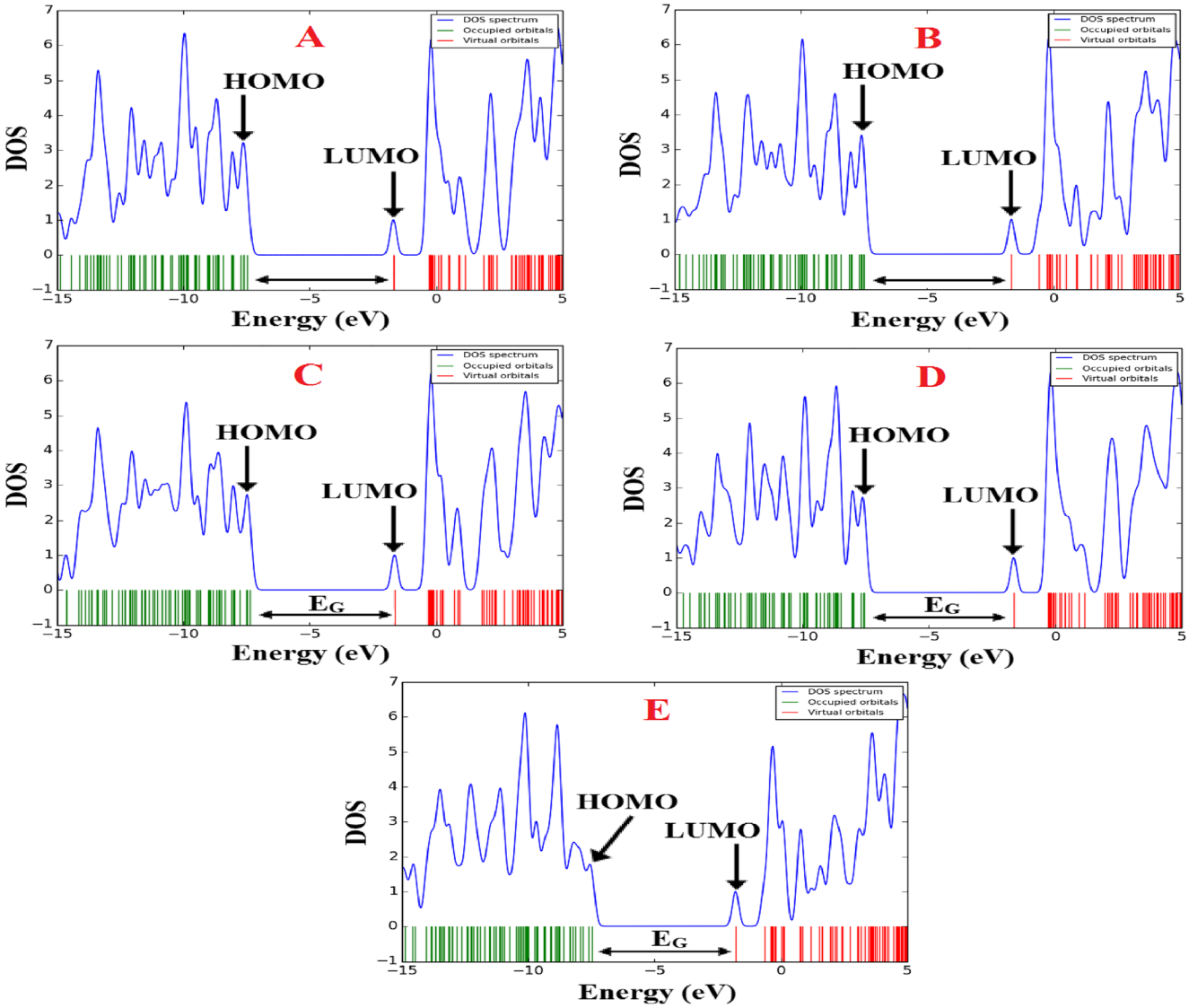

Fig. 8 DOS plots of the ZOL adsorbed on $Al_{12}N_{12}$ nanocage (models **A**–**E**)

Table 4 Calculated $E^{(2)}$ values (kcal mol^{-1}) of ZOL/$B_{12}N_{12}$ and ZOL/$Al_{12}N_{12}$ complexes

ZOL/$B_{12}N_{12}$	$LP_{O48} \rightarrow \sigma^*_{B17\text{-}N6}$	$\sigma_{N47\text{-}O48} \rightarrow \sigma^*_{B17\text{-}N3}$	$LP_{O46} \rightarrow \sigma^*_{B17\text{-}N6}$	$\sigma_{N36\text{-}H51} \rightarrow \sigma^*_{B17\text{-}N6}$	$LP_{O38} \rightarrow \sigma^*_{B17\text{-}N12}$
A	4.44	-	-	-	-
B	-	1.49	-	-	-
C	-	-	5.74	-	-
D	-	-	-	1.00	-
E	-	-	-	-	7.01
ZOL/$Al_{12}N_{12}$	$LP_{O36} \rightarrow \pi^*_{Al52\text{-}N3}$	$LP_{N35} \rightarrow \pi^*_{Al52\text{-}N3}$	$LP_{O34} \rightarrow \pi^*_{Al52\text{-}N3}$	$\sigma_{N24\text{-}C25} \rightarrow \pi^*_{Al52\text{-}N3}$	$LP_{O26} \rightarrow \pi^*_{Al52\text{-}N3}$
A	32.21	-	-	-	-
B	-	23.96	-	-	-
C	-	-	63.39	-	-
D	-	-	-	4.47	-
E	-	-	-	-	41.28

Table 5 Selected exited states, excitation energies (eV), wavelength (nm), oscillator strength (f), and relative orbital contributions of ZOL, $B_{12}N_{12}$ and $Al_{12}N_{12}$ fullerenes, and complexes

System	Excited state	λ_{max} (nm)	E (eV)	f	Configuration composition (corresponding transition orbitals)
$B_{12}N_{12}$	$S_0 \rightarrow S_{11}$	173.26	7.15	0.08	HOMO-1 → LUMO + 3 (36%)
	$S_0 \rightarrow S_{12}$	173.24	7.15	0.08	HOMO → LUMO + 3 (26%)
	$S_0 \rightarrow S_{13}$	173.20	7.15	0.08	HOMO-2 → LUMO + 4 (43%)
ZOL/$B_{12}N_{12}$					
Model **A**	$S_0 \rightarrow S_3$	220.70	5.61	0.47	HOMO → LUMO + 4 (84%)
Model **B**	$S_0 \rightarrow S_5$	223.29	5.55	0.40	HOMO → LUMO + 4 (79%)
Model **C**	$S_0 \rightarrow S_3$	219.74	5.64	0.25	HOMO → LUMO + 5 (44%)
Model **D**	$S_0 \rightarrow S_2$	227.57	5.44	0.08	HOMO → LUMO + 6 (51%)
Model **E**	$S_0 \rightarrow S_1$	232.80	5.32	0.20	HOMO → LUMO (72%)
$Al_{12}N_{12}$	$S_0 \rightarrow S_{14}$	232.52	5.33	0.02	HOMO-1 → LUMO + 7 (27%)
	$S_0 \rightarrow S_{15}$	232.45	5.33	0.02	HOMO → LUMO + 8 (30%)
	$S_0 \rightarrow S_{16}$	232.41	5.33	0.02	HOMO-5 → LUMO + 3 (25%)
ZOL/$Al_{12}N_{12}$					
Model **A**	$S_0 \rightarrow S_{13}$	257.73	4.81	0.005	HOMO-1 → LUMO + 6 (19%)
Model **B**	$S_0 \rightarrow S_{14}$	259.49	4.77	0.006	HOMO-1 → LUMO + 7 (27%)
Model **C**	$S_0 \rightarrow S_{16}$	256.69	4.83	0.007	HOMO-2 → LUMO + 9 (27%)
Model **D**	$S_0 \rightarrow S_7$	269.75	4.59	0.004	HOMO-11 → LUMO (36%)
Model **E**	$S_0 \rightarrow S_6$	279.73	4.43	0.017	HOMO → LUMO (71%)

plots of $B_{12}N_{12}$ and $Al_{12}N_{12}$ nanocages are changed after the adsorption of ZOL on nanocages. With adsorption of ZOL on two nanocages, the location of both HOMO and LUMO orbitals is changed, which displays a strong interaction between ZOL and $B_{12}N_{12}$ and $Al_{12}N_{12}$ nanocages.

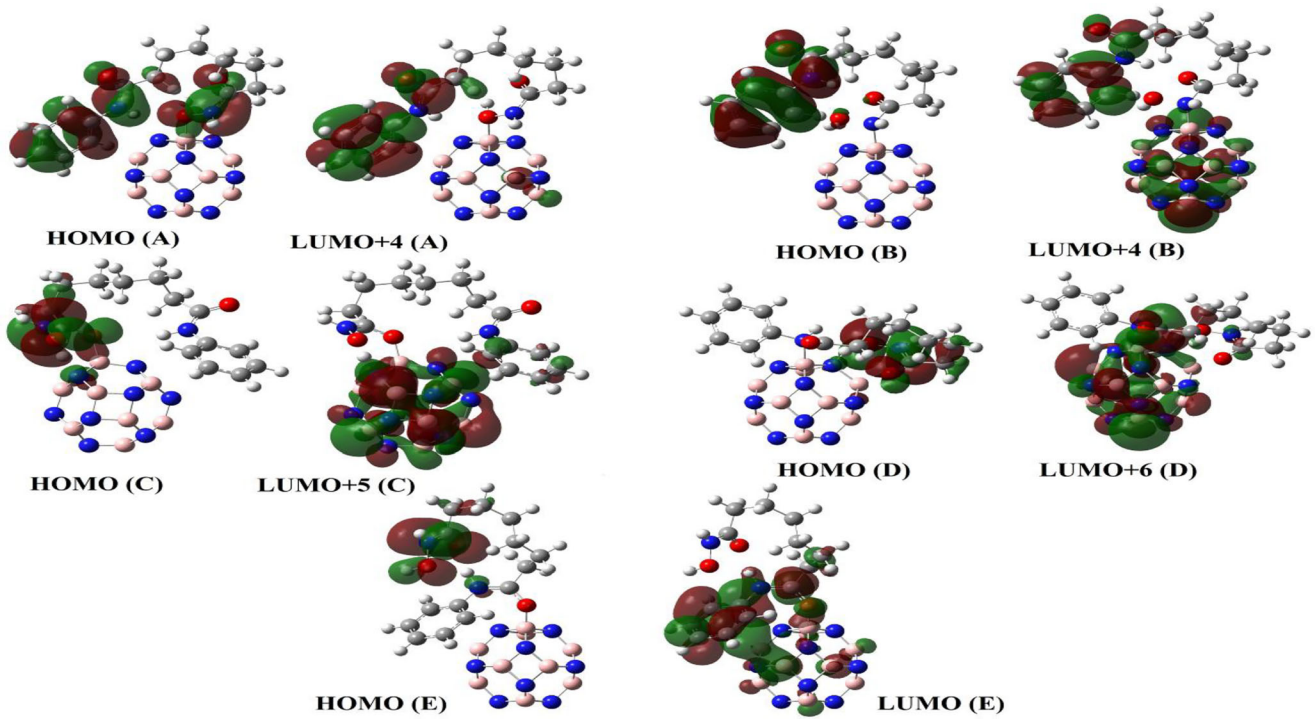

Fig. 9 Molecular orbitals participants at λ_{max} of ZOL/$B_{12}N_{12}$ complexes (**A**–**E**) calculated by TDM062-X/6-31+G* method

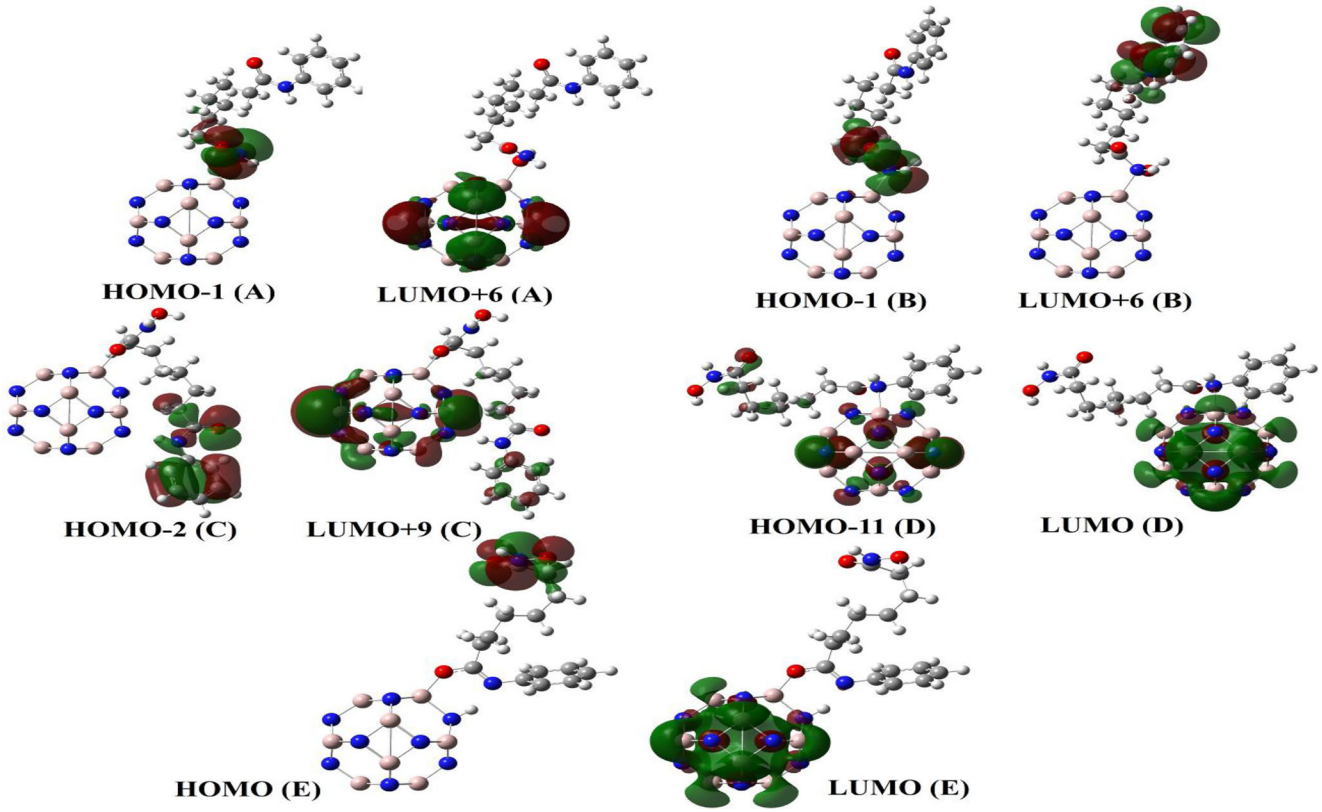

Fig. 10 Molecular orbitals participants at λ_{max} of ZOL/$Al_{12}N_{12}$ complexes (**A**–**E**) calculated by TDM062-X/6-31+G* method

NBO analysis

Natural bond orbital (NBO) analysis was performed for the study of donor-acceptor interactions during the adsorption process of ZOL on surface $B_{12}N_{12}$ and $Al_{12}N_{12}$ nanocages. The donor-acceptor interaction energy ($E^{(2)}$) is a factor to determine the stability of a molecule. There is a direct relationship between the stability of a molecule and $E^{(2)}$ values. The molecule with a higher $E^{(2)}$ value is the more stable compound. The $E^{(2)}$ values for ZOL/$B_{12}N_{12}$ and ZOL/$Al_{12}N_{12}$ complexes are reported in Table 4. According to the results of Table 4, the donor-acceptor interaction energy of the ZOL/$B_{12}N_{12}$ complexes is related to the charge transfer from the lone pair (LP) electrons of the oxygen atom and bonding orbital (σ) of the nitrogen atoms of ZOL, as a donor, to anti-bonding orbital (σ^*) of the B of $B_{12}N_{12}$ nanocage, as acceptors. The $LP_{O38} \rightarrow \sigma^*_{B17\text{-}N12}$ interaction in the **E** complex has the higher stabilization energy $E^{(2)}$ about 7.01 kcal/mol in comparison to titled interactions of the ZOL/$B_{12}N_{12}$ complexes. The $E^{(2)}$ value of the ZOL/$Al_{12}N_{12}$ complex is more than the ZOL/$B_{12}N_{12}$ complex that shows more stability of the ZOL/$Al_{12}N_{12}$ complex in comparison to the ZOL/$B_{12}N_{12}$ complex. As shown in Table 4, the important donor-acceptor interaction energies of models **A**, **B**, **C**, **E**, and ZOL/$Al_{12}N_{12}$ are related to the charge transfer between LP electrons of the oxygen and nitrogen atoms of ZOL (donor) and the anti-bonding orbital (π^*) of the Al-N bond (acceptor). In model **D**, σ orbital of the N24-C25 bond of ZOL acts as a donor and the π^* orbital of Al-N bond as acceptor ($\sigma_{N24\text{-}C25} \rightarrow \pi^*_{Al52\text{-}N3}$) with stabilization energy $E^{(2)}$ about 4.47 kcal/mol. The highest $E^{(2)}$ is observed for $LP_{O34} \rightarrow \pi^*_{Al52\text{-}N3}$ interaction of model **C** (63.39 kcal/mol).

Electronic structure and excited states

Table 5 shows the theoretical maximum absorption wavelength (λ_{max}), oscillator strength (f), vertical excitation energies (E), and orbital interactions of free $B_{12}N_{12}$ and $Al_{12}N_{12}$ nanocages and ZOL/$B_{12}N_{12}$ and ZOL/$Al_{12}N_{12}$ complexes. The λ_{max} of the free $B_{12}N_{12}$ is observed at 173.26 nm, 173.24 nm, and 173.20 nm ($f = 0.08$) in the three excited states $S_0 \rightarrow S_{11}$, $S_0 \rightarrow S_{12}$, and $S_0 \rightarrow S_{13}$ with the energy of 7.15 eV and are related to HOMO-1 → LUMO+3 (36%),

Table 6 Calculated topological parameters (in a.u) at the BCP of the selected bonds of ZOL/$B_{12}N_{12}$ and ZOL/$Al_{12}N_{12}$complexes

Complex	Bond	$\rho(r)$	$\nabla^2\rho(r)$	$H(r)$	$-G(r)/V(r)$
1	Al_{52}-O_{36}	0.0356	0.462	0.118	1.173
	N_3-H_{50}	0.0159	0.277	0.941	1.187
2	Al_{52}-N_{35}	0.0247	0.381	0.566	1.102
	N_6-H_{50}	0.0120	0.265	0.642	1.086
3	Al_{52}-O_{34}	0.0444	0.578	0.167	1.191
	N_5-H_{39}	0.0147	0.201	0.211	1.285
	N_5-H_{21}	0.0132	0.205	0.926	1.280
	N_{12}-H_{40}	0.0154	0.258	0.392	1.039
	N_{12}-H_{44}	0.0155	0.229	0.758	1.174
	N_{12}-H_{47}	0.0101	0.264	0.729	1.270
	N_6-H_{50}	0.0128	0.281	0.789	1.140
4	Al_{52}-N_{24}	0.0228	0.381	0.789	1.147
	N_{12}-H_{20}	0.0157	0.228	0.228	1.189
	N_8-H_{42}	0.0107	0.276	0.255	1.022
	N_8-H_{40}	0.0123	0.293	0.263	1.020
5	Al_{52}-O_{26}	0.0565	0.605	0.185	1.168
	N_{24}-H_{39}	0.0165	0.208	0.152	1.193
6	B_{17}-O_{48}	0.0872	0.925	−0.459	0.768
	N_4-H_{33}	0.0155	0.286	0.104	1.205
7	B_{17}-N_{47}	0.0311	0.487	−0.713	0.667
	N_3-H_{50}	0.0107	0.201	0.786	1.170
	N_3-H_{33}	0.0195	0.293	0.109	1.212
8	B_{17}-O_{46}	0.0820	0.959	−0.568	0.775
	N_{12}-H_{51}	0.0122	0.216	0.108	1.10
	O_{46}-H_{56}	0.0113	0.308	0.852	1.10
	B_{13}-C_2	0.0146	0.372	0.272	1.037
9	B_{17}-N_{36}	0.0315	0.472	−0.751	0.666
	N_6-H_{50}	0.0176	0.224	−0.358	1.165
	N_6-H_{52}	0.0117	0.221	0.135	1.170
10	B_{17}-O_{38}	0.0821	0.973	−0.564	0.779
	N_{12}-C_{26}	0.0705	0.819	0.818	1.210
	N_3-C_{27}	0.0789	0.628	0.102	1.166
	N_4-C_{25}	0.0628	0.575	0.544	1.169

HOMO → LUMO+3 (26%), and HOMO-2 → LUMO+4 (43%) transitions. The H-2 → L + 4 has the main contribution of about 43% of the total excitations. The λ_{max} of the ZOL/$B_{12}N_{12}$ complexes such as models **A**, **B**, **C**, **D**, and **E** observed at 220.70 nm (f = 0.47), 223.29 nm (f = 0.40), 219.74 nm (f = 0.25), 227.57 (f = 0.08), and 232.80 nm (f = 0.20), respectively. Figures 9 and 10 show the shape of molecular orbitals participants at λ_{max} of **A**, **B**, **C**, **D**, and **E** complexes. According to Fig. 9, the electron density of HOMO of **A** complex mainly focuses on the double bonds (-C=C-) of the aryl ring, oxygen, and nitrogen atoms of the ZOL, while the LUMO focuses on the double bonds (-C=C-) of the aryl ring and oxygen atom of one of the carbonyl groups.

The λ_{max} of the free $Al_{12}N_{12}$ is observed at 232.52 nm, 232.45 nm, and 232.41 nm (f = 0.02) in the three excited states $S_0 \rightarrow S_{14}$, $S_0 \rightarrow S_{15}$, and $S_0 \rightarrow S_{16}$ with energy of 5.33 eV and is related to H-1 → L + 7 (27%), H → L + 8 (30%), and H-5 → L + 3 (25%) transitions. The H → L + 8 has the main contribution about 30% of the total excitations. TD-DFT results of the ZOL/$Al_{12}N_{12}$ complexes show that the λ_{max} of models **A**, **B**, **C**, **D**, and **E** is observed at 257.73 nm (f = 0.005), 259.49 nm (f = 0.006), 256.69 nm (f = 0.007), 269.75 (f = 0.004), and 279.73 nm (f = 0.017).

According to TD-DFT results, the λ_{max} increases during the adsorption process of ZOL on nanocages that can be considered as a *bathochromic shift (redshift)*.

QTAIM, ELF, and LOL analysis

To obtain more details about the nature of intermolecular interactions, the quantum theory of atoms in molecule (QTAIM) analysis was performed at the bond critical point (BCP). The molecular graphs of ZOL/$B_{12}N_{12}$ and ZOL/$Al_{12}N_{12}$ complexes are shown in Fig. 11. Based on this figure, there are several intermolecular hydrogen bondings between nitrogen, oxygen atoms of ZOL, and the hydrogen atom of nanocages. The topological analysis of the complexes at the BCP is reported in Table 6. The values of electron density ($\rho(r)$) describe the strength of a chemical bond, in which the higher value of $\rho(r)$ shows the stronger interaction. Calculated values of $\rho_{B\text{-}O}$ are greater than $\rho_{Al\text{-}O}$, $\rho_{Al\text{-}N}$, $\rho_{B\text{-}N}$, $\rho_{N\text{-}H}$, $\rho_{O\text{-}H}$, $\rho_{B\text{-}C}$, and $\rho_{N\text{-}C}$, which reveals that the boron atom of $B_{12}N_{12}$ has the most interaction with oxygen atoms of ZOL. The negative values of the Laplacian of electron density ($\nabla^2\rho(r)$) and total energy density ($H(r)$) indicate the strong interactions, whereas the positive values of $\nabla^2\rho(r)$ and the negative values of $H(r)$ indicate the medium interactions [48]. In the case of weak interactions, $\nabla^2\rho(r)$ and $H(r)$ values are positive. According to Table 6, the calculated $\nabla^2\rho(r)$ and $H(r)$ values of Al-O, B-N Al-N, N-H, O-H, B-C, and N-C bonds are positive, showing weak interactions. In contrast, the $\nabla^2\rho(r)$ values of B-O bonds are positive, whereas $H(r)$ values are negative, showing intermediate interactions.

The ratio of kinetic energy density ($G(r)$) to the potential energy density (V(r)) values is also used to determine the nature of interactions, such that 0.5 <− $G(r)/V(r)$ <0, 1<− $G(r)/V(r)$<0.5, and − $G(r)/V(r)$ >1 indicates covalent, partial covalent, and non-covalent (electrostatic, Van der Walls, and hydrogen bonding) interactions, respectively [49]. According

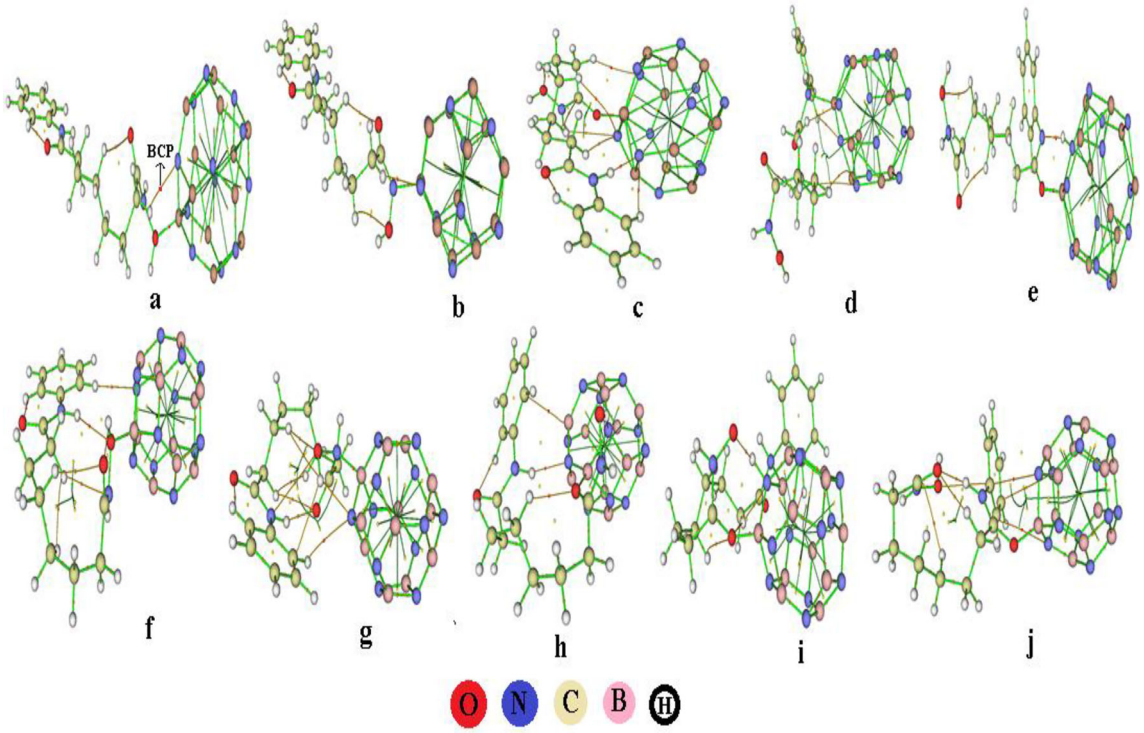

Fig. 11 Molecular graphs of **a** complex 1, **b** complex 2, **c** complex 3, **d** complex 4, **e** complex 5, **f** complex 6, **g** complex 7, **h** complex 8, **i** complex 9, and **j** complex 10

to Table 6, calculated $-G(r)/V(r)$ values of Al-N, Al-O, N-H, O-H, B-C, and N-C bonds are greater than unit, showing non-covalent interactions, whereas these values for B-O and B-N bonds are between 0.5 and 1, confirming the partial covalent interactions.

Electron Localization Function (ELF) and Localized Orbital Locator (LOL) analyses [50, 51] of studied complexes have been also performed, and the corresponding maps are visualized in Fig. 12. High and low ELF and LOL values indicate covalent and non-covalent interactions, respectively. According to Fig. 11, the LOL and ELF values of Al-O and Al-N bonds are low in the region between reactive atoms of ZOL (oxygen and nitrogen) and aluminum atom of $Al_{12}N_{12}$, confirming the non-covalent interactions between them. On the contrary, the high ELF and LOL values between reactive atoms of the ZOL (oxygen and nitrogen) and boron atom of $B_{12}N_{12}$ indicate that these interactions are an electrostatic and partially covalent character.

Conclusion

In this study, the adsorption of ZOL molecule on the surfaces of $B_{12}N_{12}$ $Al_{12}N_{12}$ nanocages was investigated using DFT calculations. It is found that ZOL drug strongly interacted with surfaces of $B_{12}N_{12}$ and $Al_{12}N_{12}$ nanocages due to the large negative E_{ads}, ΔG, and ΔH values. The change of D_M shows a charge transfer between ZOL drug and $B_{12}N_{12}$ and $Al_{12}N_{12}$ nanocages, and the polarization in complexes is increased. The $B_{12}N_{12}$ nanocage with a higher change in the E_G is the better candidate as a suitable electrochemical sensor rather than the $Al_{12}N_{12}$ nanocage. Furthermore, we found that the adsorption of the ZOL from the head of N24 atom (model **B**) on the surface of $B_{12}N_{12}$ nanocage is more considerable in comparison to other models due to the lower E_G (6.35 eV). The TD-DFT calculations display that the adsorption of ZOL on nanocages can shift λ_{max} values to longer wavelengths (redshift). Also, the analysis of UV spectra of the ZOL adsorbed over $B_{12}N_{12}$ and $Al_{12}N_{12}$ fullerene can be considered as a *bathochromic shift (redshift)*. The high ELF and LOL values between reactive atoms of ZOL (oxygen and nitrogen) and boron atom of $B_{12}N_{12}$ indicate that these interactions are an electrostatic and partially covalent character. According to the changes in the $B_{12}N_{12}$ and $Al_{12}N_{12}$ nanocages, we suggest the $B_{12}N_{12}$ nanocage as the best adsorbent and drug delivery system for the ZOL molecule. We hope that the results of our calculations can be useful for designing an appropriate and novel carrier for the delivery of the Zolinza drug.

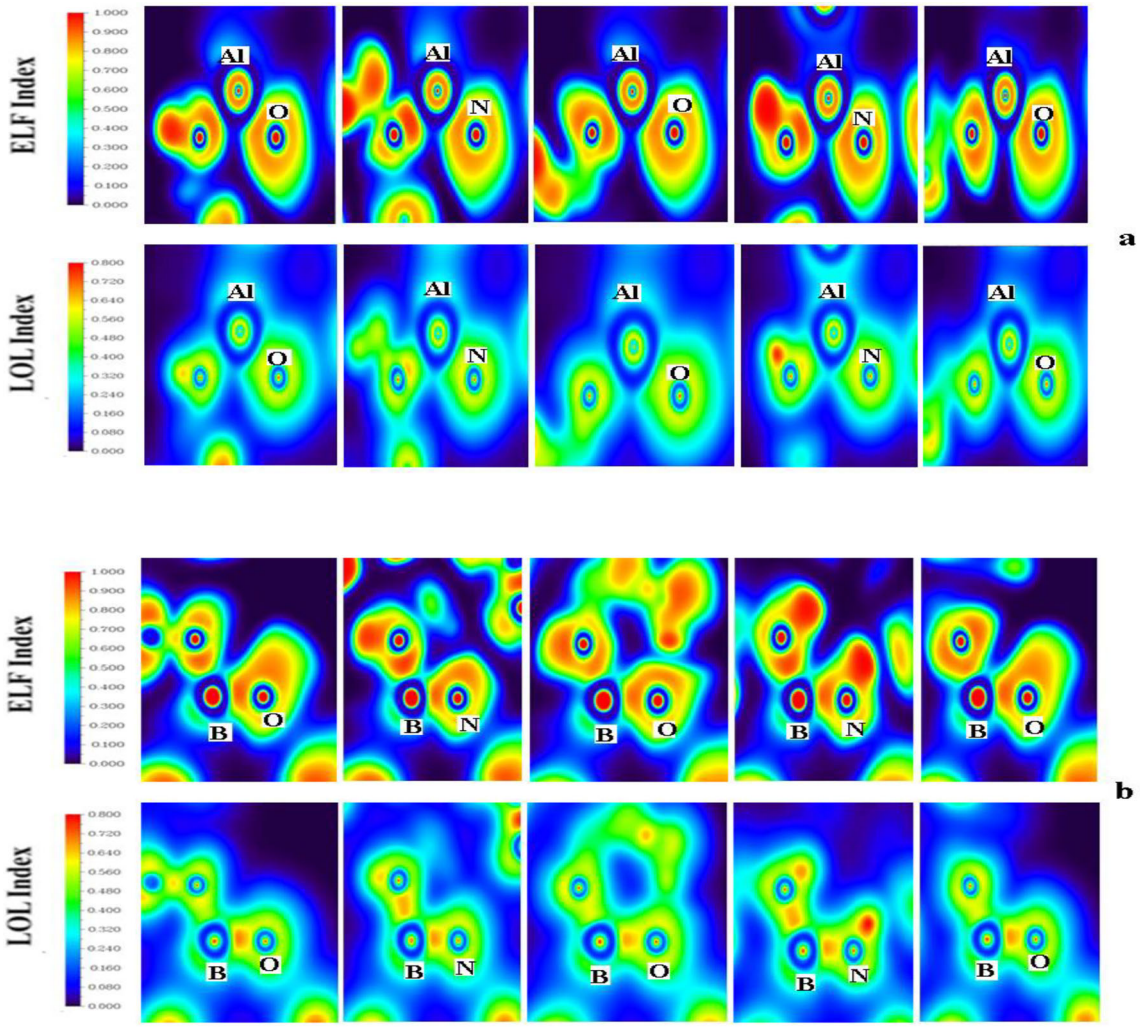

Fig. 12 ELF and LOL maps of oxygen and nitrogen atoms interacting with **a** $B_{12}N_{12}$ and **b** $Al_{12}N_{12}$ nanocages

Authors' contribution Masoome Sheikhi: project administration, supervision, writing (original draft), writing (review and editing), investigation, and revision.

Yavar Ahmadi: resources, methodology, and software.

Sadegh Kaviani: visualization, writing (original draft), and methodology.

Siyamak Shahab: writing (review and editing), data curation, and software.

Data availability Our manuscript has no associated data or the data will not be deposited.

Compliance with ethical standards

Conflict of interest The authors declare that they have no conflict of interest.

Consent to participate We understand that this manuscript and associated personal data will be shared with Research Square for the delivery of the author dashboard.

Consent to publish We agree to the publication of the accepted manuscript.

References

1. Jones PA, Issa JPJ, Baylin S (2016) Targeting the cancer epigenome for therapy. Nat Rev Genet 17:630–641
2. Nakagawa M, Oda Y, Eguchi T, Aishima S-I, Yao T, Hosoi F, Basaki Y, Ono M, Kuwano M, Tanaka M, Tsuneyoshi M (2007) Expression profile of class I histone deacetylases in human cancer tissues. Oncol Rep 18:769–774
3. Eckschlager T, Plch J, Stiborova M, Hrabeta J (2017) Histone deacetylase inhibitors as anticancer drugs. Int J Mol Sci 18:1–25
4. Xu WS, Parmigiani RB, Marks PA (2007) Histone deacetylase inhibitors: molecular mechanisms of action. Oncogene 26:5541–5552
5. Uehara N, Yoshizawa K, Tsubura A (2012) Vorinostat enhances protein stability of p27 and p21 through negative regulation of Skp2 and Cks1 in human breast cancer cells. Oncol Rep 28:105–110
6. Dias JNR, Aguiar SI, Pereira DM, André AS, Gano L, Correia JDG et al (2018) The histone deacetylase inhibi tor panobinostat is a potent antitumor agent in canine diffuse large B-cell lymphoma. Oncotarget 9:28586–28598
7. Elshafae SM, Kohart NA, Altstadt LA, Dirksen WP, Rosol TJ (2017) The effect of a histone deacetylase inhibitor (AR-42) on canine prostate cancer growth and metastasis. Prostate 793:776–793

8. Cohen LA, Powers B, Amin S, Desai D (2004) Treatment of canine haemangiosarcoma with suberoylanilide hydroxamic acid, a histone deacetylase inhibitor. Vet Comp Oncol 2:243–248
9. Spange S, Wagner T, Heinzel T, Kramer OH (2009) Acetylation of non-histone proteins modulates cellular signalling at multiple levels. Int J Biochem Cell Biol 41:185–198
10. Bolden JE, Shi W, Jankowski K, Kan CY, Cluse L, Martin BP, MacKenzie KL, Smyth GK, Johnstone RW (2013) HDAC inhibitors induce tumor-cell-selective pro-apoptotic transcriptional responses. Cell Death Dis 4:e519
11. Kavanaugh SA, White LA, Kolesar JM (2010) Vorinostat: a novel therapy for the treatment of cutaneous T-cell lymphoma. Am J Heal Pharm 67:793–797
12. Yang YT, Balch C, Kulp SK, Mand MR, Nephew KP, Chen CS (2009) A rationally designed histone deacetylase inhibitor with distinct antitumor activity against ovarian cancer. Neoplasia 11:552–563
13. Walker T, Mitchell C, Park MA, Yacoub A, Graf M, Rahmani M, Houghton PJ, Voelkel-Johnson C, Grant S, Dent P (2009) Sorafenib and vorinostat kill colon cancer cells by CD95-dependent and independent mechanisms. Mol Pharmacol 76:342–355
14. Munster PN, Lacevic M, Schmitt M, Bicaku E, Marchion D, Stephens A, Sullivan L, Minton S (2008) (ASCO annual meeting proceedings). J Clin Oncol 1:3501
15. Owonikoko TK, Ramalingam SS, Kanterewicz B, Balius T, Belani CP, Hershberger PA (2009) Vorinostat increases carboplatin and paclitaxel activity in nonsmall cell lung cancer cells. Int J Cancer 126:743–755
16. Trédaniel J, Descourt R, Moro-Sibilot D, Misset J, Gachard E, Garcia-Vargas J, Roben E, Zalcman G (2009) Vorinostat in combination with gemcitabine and cisplatinum in patients with advanced non-smallcell lung cancer (NSCLC): a phase I dose escalation study. (ASCO annual meeting). J Clin Oncol 27:8049
17. Hughes B (2010) 2009 FDA drug approvals. Nat Rev Drug Discov 9:89–92
18. Mann BS, Johnson JR, Cohen MH, Justice R, Pazdur R (2007) FDA approval summary: vorinostat for treatment of advanced primary cutaneous T-cell lymphoma. Oncologist 12:1247–1252
19. Lu H, Wang J, Wang T, Zhong J, Bao Y, Hao H (2016) Recent progress on nanostructures for drug delivery applications. J Nanomater 2016:1–12
20. Farokhzad OC, Langer R (2009) Impact of nanotechnology on drug delivery. ACS Nano 3:16–20
21. Sahoo SK, Parveen S, Panda JJ (2007) The present and future of nanotechnology in human health care. Nanomed Nanotechnol 3:20–31
22. Peer D, Karp JM, Hong S, Hong S, Margalit R, Langer R (2007) Nanocarriers as an emerging platform for cancer therapy. Nat Nanotechnol 2:751–760
23. Jabr-Milane LS, van Vlerken LE, Yadav S, Amiji MM (2008) Multi-functional nanocarriers to overcome tumor drug resistance. Cancer Treat Rev 34:592–602
24. Mirsa R, Acharya S, Sahoo SK (2010) Cancer nanotechnology: application of nanotechnology in cancer therapy. Drug Discov Today 15:842–850
25. Sheikhi M, Shahab S, Alnajjar R, Ahmadianarog M, Kaviani S (2019) Investigation of adsorption tyrphostin AG528 anticancer drug upon the CNT (6, 6-6) nanotube: a DFT study. Curr Mol Med 19:91–104
26. Sheikhi M, Shahab S, Khaleghian M, Kumar R (2018) Interaction between new anti-cancer drug syndros and CNT (6, 6-6) nanotube for medical applications: geometry optimization, molecular structure, spectroscopic (NMR, UV/Vis, excited state), FMO, MEP and HOMO-LUMO investigation. Appl Surf Sci 434:504–513
27. Sheikhi M, Shahab S, Khaleghian M, Hajikolaee FH, Balakhanava I, Alnajjar R (2018) Adsorption properties of the molecule resveratrol on CNT (8, 0-10) nanotube: geometry optimization, molecular structure, spectroscopic (NMR, UV/Vis, excited state), FMO, MEP and HOMO-LUMO investigations. J Mol Struct 1160:479–478
28. Zhu YC, Bando Y, Yin LW, Golberg D (2004) Hollow boron nitride (BN) nanocages and BN-nanocage-encapsulated nanocrystals. Chem Eur J 10:3667–3672
29. Oku T, Nishiwaki A, Narita I (2004) Formation and atomic structure of $B_{12}N_{12}$ nanocage clusters studied by mass spectrometry and cluster calculation. Sci Technol Adv Mater 5:635–638
30. Liu C, Hu Z, Wu Q, Wang X, Chen Y, Zhu J (2006) Controllable synthesis of one-dimensional aluminum nitride nanostructures through vapor-solid epitaxial growth. J Nanoelectron Optoelectron 1:114–118
31. Akiyama M, Morofuji Y, Kamohara T, Nishikubo K, Ooishi Y, Tsubai M, Fukuda O, Ueno N (2007) Preparation of oriented aluminum nitride thin films on polyimide films and piezoelectric response with high thermal stability and flexibility. Adv Funct Mater 17:458–462
32. Padash R, Sobhani-Nasab A, Rahimi-Nasrabadi M, Mirmotahari M, Ehrlich H, Rad AS, Peyravi M (2018) Is it possible to use $X12Y12$ (X = Al, B, and Y = N, P) nanocages for drug-delivery systems? A DFT study on the adsorption property of 4-aminopyridine drug. Appl Phys A Mater Sci Process 124:582
33. Wu HS, Zhang FQ, Xu XH, Zhang CJ, Jiao H (2003) Geometric and energetic aspects of aluminum nitride cages. J Phys Chem A 107:204–209
34. Vessally E, Esrafili MD, Nurazar R, Nematollahi P, Bekhradnia A (2017) A DFT study on electronic and optical properties of aspirin-functionalized $B_{12}N_{12}$ fullerene-like nanocluster. Struct Chem 28:735–748
35. Bahrami A, Qarai MB, Hadipour NL (2017) The electronic and structural responses of $B_{12}N_{12}$ nanocage toward the adsorption of some nonpolar X_2molecules: X=(Li, Be, B, N, O, F, Cl, Br, I): a DFT approach. Comput Theor Chem 1108:63–69
36. Yourdkhani S, Korona T, Hadipour NL (2015) Structure and energetics of complexes of $B_{12}N_{12}$ with hydrogen halides-SAPT (DFT) and MP2 study. J Phys Chem A 119:6446–6467
37. Shokuhi Rad A, Zareyee D, Pouralijan Foukolaei V, Kamyab Moghadas B, Peyravi M (2016) Study on the electronic structure of $Al_{12}N_{12}$ and $Al_{12}P_{12}$ fullerene-like nano-clusters upon adsorption of CH_3F and CH_3Cl. Mol Phys 114:3143–3149
38. Yahyaei H, Sharifi S, Shahab S, Sheikhi M, Ahmadianarog M (2020) Theoretical study of adsorption of solriamfetol drug on surface of the $B_{12}N_{12}$ fullerene: a DFT/TD-DFT approach. Lett Org Chem. https://doi.org/10.2174/1570178617999200818104322
39. Frisch MJ, Trucks GW, Schlegel HB, Scuseria GE, Robb MA, Cheeseman JR, Scalmani G, Barone V, Mennucci B, Petersson GA, Nakatsuji H, Caricato M, Li X, Hratchian HP, Izmaylov AF, Bloino J, Zheng G, Sonnenberg JL, Hada M, Ehara M, Toyota K, Fukuda R, Hasegawa J, Ishida M, Nakajima T, Honda Y, Kitao O, Nakai H, Vreven T, Montgomery JA, Peralta JE, Ogliaro F, Bearpark M, Heyd JJ, Brothers E, Kudin KN, Staroverov VN, Kobayashi R, Normand J, Raghavachari K, Rendell A, Burant JC, Iyengar SS, Tomasi J, Cossi M, Rega N, Millam JM, Klene M, Knox JE, Cross JB, Bakken V, Adamo C, Jaramillo J, Gomperts R, Stratmann RE, Yazyev O, Austin AJ, Cammi R, Pomelli C, Ochterski JW, Martin RL, Morokuma K, Zakrzewski VG, Voth GA, Salvador P, Dannenberg JJ, Dapprich S, Daniels AD, Farkas O, Foresman JB, Ortiz JV, Cioslowski J, Fox DJ (2009) Gaussian 09 revision A02. Gaussian, Inc., Wallingford
40. Tomasi J, Mennucci B, Cammi R (2005) Quantum mechanical continuum solvation models. Chem Rev 105:2999–3093
41. Weinhold F, Landis CR (2001) Natural bond orbitals and extensions of localized. Chem Educ Res Pract 2:91–104

42. Frisch A, Nielson AB, Holder AJ (2000) GAUSSVIEW user manual. Gaussian Inc., Pittsburgh, PA
43. O'Boyle N, Tenderholt A, Langner K (2008) cclib: a library for package–independent computational chemistry algorithms. J Comput Chem 29:839–845
44. Runge E, Gross EKU (1984) Density-functional theory for time-dependent systems. Phys Rev Lett 52:997–1000
45. Shyam Kumar Vinod P, Raghavendra V, Subramanian V (2016) Bader's theory of atoms in molecules (AIM) and its applications to chemical bonding. J Chem Sci 128:1527–1536
46. Lu T, Chen F (2012) Multiwfn: a multifunctional wave function analyzer. J Comput Chem 33:580–592
47. Baei MT, Soltani A, Torabi P, Hashemian S (2015) $Al_{12}N_{12}$ nanocage as potential adsorbent for removal of acetone from environmental systems. Monatsh Chem 146:891–896
48. Grabowski SJ (2006) Theoretical studies of strong hydrogen bonds. Annu Rep C 102:131–165
49. Khavani M, Izadyar M, Housaindokht MR (2015) DFT investigation and molecular dynamic simulation on the selective complexation of cis-cyclic nanopeptides with alkaline earth metal ions. Sensors Actuators B Chem 221:1120–1129
50. Tsirelson V, Stash A (2002) Determination of the electron localization function from electron density. Chem Phys Lett 351:142–148
51. Jacobsen H (2008) Localized-orbital locator (LOL) profiles of chemical bonding. Can J Chem 86:695–702

Terms and Conditions

Springer Nature journal content, brought to you courtesy of Springer Nature Customer Service Center GmbH (“Springer Nature”).
Springer Nature supports a reasonable amount of sharing of research papers by authors, subscribers and authorised users (“Users”), for small-scale personal, non-commercial use provided that all copyright, trade and service marks and other proprietary notices are maintained. By accessing, sharing, receiving or otherwise using the Springer Nature journal content you agree to these terms of use (“Terms”). For these purposes, Springer Nature considers academic use (by researchers and students) to be non-commercial.
These Terms are supplementary and will apply in addition to any applicable website terms and conditions, a relevant site licence or a personal subscription. These Terms will prevail over any conflict or ambiguity with regards to the relevant terms, a site licence or a personal subscription (to the extent of the conflict or ambiguity only). For Creative Commons-licensed articles, the terms of the Creative Commons license used will apply.
We collect and use personal data to provide access to the Springer Nature journal content. We may also use these personal data internally within ResearchGate and Springer Nature and as agreed share it, in an anonymised way, for purposes of tracking, analysis and reporting. We will not otherwise disclose your personal data outside the ResearchGate or the Springer Nature group of companies unless we have your permission as detailed in the Privacy Policy.
While Users may use the Springer Nature journal content for small scale, personal non-commercial use, it is important to note that Users may not:

1. use such content for the purpose of providing other users with access on a regular or large scale basis or as a means to circumvent access control;
2. use such content where to do so would be considered a criminal or statutory offence in any jurisdiction, or gives rise to civil liability, or is otherwise unlawful;
3. falsely or misleadingly imply or suggest endorsement, approval , sponsorship, or association unless explicitly agreed to by Springer Nature in writing;
4. use bots or other automated methods to access the content or redirect messages
5. override any security feature or exclusionary protocol; or
6. share the content in order to create substitute for Springer Nature products or services or a systematic database of Springer Nature journal content.

In line with the restriction against commercial use, Springer Nature does not permit the creation of a product or service that creates revenue, royalties, rent or income from our content or its inclusion as part of a paid for service or for other commercial gain. Springer Nature journal content cannot be used for inter-library loans and librarians may not upload Springer Nature journal content on a large scale into their, or any other, institutional repository.
These terms of use are reviewed regularly and may be amended at any time. Springer Nature is not obligated to publish any information or content on this website and may remove it or features or functionality at our sole discretion, at any time with or without notice. Springer Nature may revoke this licence to you at any time and remove access to any copies of the Springer Nature journal content which have been saved.
To the fullest extent permitted by law, Springer Nature makes no warranties, representations or guarantees to Users, either express or implied with respect to the Springer nature journal content and all parties disclaim and waive any implied warranties or warranties imposed by law, including merchantability or fitness for any particular purpose.
Please note that these rights do not automatically extend to content, data or other material published by Springer Nature that may be licensed from third parties.
If you would like to use or distribute our Springer Nature journal content to a wider audience or on a regular basis or in any other manner not expressly permitted by these Terms, please contact Springer Nature at

onlineservice@springernature.com